Cellobiose consumption uncouples extracellular glucose sensing and glucose metabolism in *Saccharomyces cerevisiae*

Kulika Chomvong[1], Daniel I. Benjamin[2], Daniel K. Nomura[2] and Jamie H.D. Cate[3,4,5,#]

[1]Department of Plant and Microbial Biology, University of California, Berkeley, CA 94720

[2]Department of Nutritional Sciences and Toxicology, University of California, Berkeley, CA 94720

[3]Department of Molecular and Cell Biology, University of California, Berkeley, CA 94720

[4]Department of Chemistry, University of California, Berkeley, CA 94720

[5]Physical Biosciences Division, Lawrence Berkeley National Laboratory, Berkeley, CA 94720

[#]Corresponding author (email: jcate@lbl.gov)

KC: kchomv@gmail.com

DIB: dbenjami@stanford.edu

DKN: dnomura@berkeley.edu

JHDC: jcate@lbl.gov

Running title: ATP and optimal glucose consumption

23 Final character count: 46,908

24 Keywords: cellobiose/glucose sensors/metabolomics/PMA1

25

26 **Abstract**

27

28 Glycolysis is central to energy metabolism in most organisms, and is highly
29 regulated to enable optimal growth. In the yeast *Saccharomyces cerevisiae*, feedback
30 mechanisms that control flux through glycolysis span transcriptional control to
31 metabolite levels in the cell. Using a cellobiose consumption pathway, we decoupled
32 glucose sensing from carbon utilization, revealing new modular layers of control that
33 induce ATP consumption to drive rapid carbon fermentation. Alterations of the beta
34 subunit of phosphofructokinase (*PFK2),* H^+-plasma membrane ATPase (*PMA1),* and
35 glucose sensors *(SNF3, RGT2)* revealed the importance of coupling extracellular
36 glucose sensing to manage ATP levels in the cell. Controlling the upper bound of
37 cellular ATP levels may be a general mechanism used to regulate energy levels in cells,
38 via a regulatory network that can be uncoupled from ATP concentrations under
39 perceived starvation conditions.

40 **Importance**

41 Living cells are fine-tuned through evolution to thrive in their native environments.
42 Genome alterations to create organisms for specific biotechnological applications may
43 result in unexpected and undesired phenotypes. We used a minimal synthetic biological
44 system in the yeast *Saccharomyces cerevisiae* as a platform to reveal novel
45 connections between carbon sensing, starvation conditions and energy homeostasis.
46
47

47

48 ## Introduction

49 Most microorganisms favor glucose as their primary carbon source, as reflected
50 in their genetic programs hard-wired for this preference. Central to carbon metabolism is
51 glycolysis, which is finely tuned to the dynamic state of the cell due to the fact that
52 glycolysis first consumes ATP before generating additional ATP equivalents. To avoid
53 catastrophic depletion of ATP, the yeast *Saccharomyces cerevisiae* has evolved a
54 transient ATP hydrolysis futile cycle coupled to gluconeogenesis (1). Glycolysis in yeast
55 is also tightly coupled to glucose transport into the cell, entailing three extracellular
56 glucose sensing mechanisms and at least one intracellular glucose signaling pathway
57 (2).

58 Synthetic biology and metabolic engineering of yeast holds promise to convert
59 this microorganism into a “cell factory” to produce a wide range of chemicals derived
60 from renewable resources or those unattainable through traditional chemical routes.
61 However, many applications require tapping into metabolites involved in central carbon
62 metabolism, a daunting challenge as living cells have numerous layers of feedback
63 regulation that fine-tune growth to changing environments. Cellular regulation evolved
64 intricate networks to maintain and ensure cell survival. For example, *S. cerevisiae* has
65 evolved to rapidly consume high concentrations of glucose through fermentation, while
66 repressing the expression of other carbon consumption pathways, an effect termed
67 glucose repression. When perturbed genetically, regulatory networks such as those in
68 glucose repression often generate undesirable or unexpected phenotypes.

69 For yeast to be useful in producing large volumes of renewable chemicals or
70 biofuels, it will be important to expand its carbon utilization to include multiple sugars in
71 the plant cell wall. One promising approach that helps overcome glucose repression
72 and allows simultaneous utilization of different sugars is cellobiose consumption (3).
73 Cellobiose is a disaccharide with two units of glucose linked by a ß-1,4 glycosidic bond.
74 Cellobiose consumption using a minimal additional pathway in yeast—a cellodextrin
75 transporter (CDT-1) and intracellular ß-glucosidase (4)–avoids glucose repression by
76 importing carbon in the form of cellobiose instead of glucose. The cellodextrin
77 transporter allows cellobiose to enter the cell where it is hydrolyzed to glucose and
78 consumed via the native glycolytic consumption pathway. By moving glucose production
79 into the cell, the *Neurospora crassa*-derived cellobiose consumption pathway is nearly
80 the minimal synthetic biological module imaginable in *S. cerevisiae*, comprised of just
81 two genes. Nevertheless, in *S. cerevisiae* the cellobiose consumption pathway is inferior
82 to consumption of extracellular glucose in terms of rate and results in a prolonged lag
83 phase (5). Previous efforts to understand the impact of cellobiose consumption on the
84 physiology of *S. cerevisiae* using transcriptional profiling revealed that cellobiose
85 improperly regulates mitochondrial activity and amino acid biosynthesis, both of which
86 are tightly coupled to the transition from respiration to fermentation (5).
87 Since glycolytic enzymes are regulated mostly at the post-transcriptional level (6),
88 we probed cellobiose consumption in *S. cerevisiae* at the metabolite level. We found
89 that key metabolites in glycolysis are highly imbalanced, leading to low flux through
90 glycolysis and slow fermentation. We also found that excess ATP levels drive the

91 imbalance, and identified a new potential regulatory role of glucose sensors in cellular
92 ATP homeostasis.
93

94 Results

95

96 Metabolite profiling of cellobiose utilizing *S. cerevisiae*

97 *S. cerevisiae* cells engineered with the cellobiose consumption pathway exhibits
98 a prolonged lag phase, with decreased growth and carbon consumption rates in
99 comparison to when glucose is provided (Figure S1A) (5). We hypothesized that
100 cellobiose consumption results in an ATP deficit in glycolysis relative to glucose, due to
101 the fact that the cellodextrin transporter (CDT-1) in the cellobiose utilizing pathway is a
102 proton symporter, requiring ATP hydrolysis for cellobiose uptake (7). Moreover, under
103 anaerobic conditions, ATP production is limited to substrate-level phosphorylation,
104 further restricting ATP availability. We measured the steady-state concentrations of ATP
105 and other metabolites in central carbon metabolism in yeast fermenting cellobiose
106 compared to glucose. Of the 48 compounds analyzed, the abundance of 25 compounds
107 was significantly different between cellobiose and glucose-fed samples (Figure S1B).
108 Surprisingly, ATP levels increased by 6-fold in the cellobiose grown cells (Figure 1A).
109 The relative abundance of compounds in glycolysis—fructose 6-phosphate (F6P),
110 glucose 6-phosphate (G6P), glucose and pyruvate—increased by 444-, 81-, 7- and 3-
111 fold, respectively, while that of phosphoenolpyruvate (PEP) decreased by 2-fold (Figure
112 1A, B). These results suggest that the yeast cells underwent drastic physiological

113 changes, reflected in metabolite levels, when cellobiose was provided in place of
114 glucose.
115
116 **Phosphofructokinase-1 inhibition by excess ATP**
117 Given the dramatic buildup of glucose, G6P and F6P intermediates prior to the
118 phosphofructokinase (*PFK1*) reaction in glycolysis (Figure 1B, 2A), we reasoned that
119 Pfk1 might be a major bottleneck in cellobiose consumption. Pfk1 catalyzes the
120 phosphorylation of F6P, using one ATP and yielding fructose 1,6-bisphosphate
121 (F1,6BP) as a product. As the second committed step in glycolysis, Pfk1 is heavily
122 regulated—with ATP acting as an allosteric inhibitor and AMP and fructose 2,6-
123 bisphosphate serving as activators (8-10).
124 To test whether allosteric inhibition of Pfk1 by ATP limited cellobiose
125 fermentation, a mutation in Pfk1 that makes the enzyme ATP-insensitive (P722L in the
126 Pfk1 beta subunit, note the original publication referred to this mutation as P728L (11))
127 was introduced into the chromosomally encoded *PFK1* gene (mutation here termed
128 *pfk1m*) in the cellobiose utilizing strain. This mutation was previously shown to reduce
129 ATP inhibition but also AMP and fructose 2,6-bisphosphate activation of Pfk1 in *S.*
130 *cerevisiae* (11). We chose this mutation over an ATP-insensitive, AMP/F2,6BP-sensitive
131 mutant phosphofructokinase (10) because the latter's phenotype has not been
132 evaluated in *S. cerevisiae*. High initial cell densities were used hereafter, as the focus of
133 this study is sugar consumption rather than growth.
134 Consistent with allosteric inhibition of Pfk1 by ATP, the cellobiose consumption
135 efficiency (E_c) of the *pfk1m* strain increased by 33% in comparison to the strain with

136 wild-type Pfk1 (Figure 2B). In these high cell densities, negligible changes in growth rate
137 were observed (Figure 2C). The relative abundance of G6P and F1,6BP decreased by
138 47% and 34%, respectively, while that of ATP remained relatively unchanged (Figure
139 2D). The unchanged ATP level was expected as the ATP requirement for the cellobiose
140 consumption pathway was likely offset by the ATP generated as part of carbon
141 metabolism. These results indicate that the 6-fold increase in cellular ATP
142 concentrations allosterically inhibited Pfk1, resulting in accumulation of glucose, G6P
143 and F6P, which eventually slowed down cellobiose consumption.
144

145 **Limited activity of plasma membrane ATPase**

146 Although the *pfk1m* strain partially increased the rate of cellobiose fermentation,
147 cellular ATP remained elevated relative to glucose fermentation. It is unlikely that ATP
148 production was the cause of the difference, as fermentation is limited to substrate-level
149 phosphorylation under anaerobic conditions regardless of carbon source. We therefore
150 tested whether the activity of one of the major ATP sinks in yeast, the plasma
151 membrane ATPase (Pma1) was responsible for the ATP buildup. Pma1 hydrolyzes 25-
152 40% of cellular ATP in yeast (12) and is heavily regulated by glucose (13).

153 A constitutively active mutant form of *PMA1* (*pma1-Δ916*, here abbreviated *pt*)
154 (14) was introduced into the endogenous *PMA1* locus in the cellobiose utilizing strain.
155 This mutation results in high Pma1 ATPase activity even in carbon starvation conditions
156 (14). The E_c of the *pt* strain was 4 times that of the control (Figure 2B), whereas the
157 growth rate of *pt* strain was only slightly faster than the Pma1 WT strain (Figure 2C). As
158 expected, we observed a 66% decrease in cellular ATP levels in the *pt* strain in

159 comparison to the wild-type control (WT, i.e. cellobiose pathway only) (Figure 2D). In
160 addition, the concentrations of G6P and F1,6BP decreased by 58% and 93%,
161 respectively, relative to strains expressing wild-type *PMA1*. Notably, these
162 concentrations dropped more than when the ATP-insensitive *PFK1* mutant was
163 introduced (Figure 2D). These results suggest that increased Pma1 ATPase activity
164 improved cellobiose fermentation. We hypothesize that the drastic decrease in F1,6BP
165 level and the fast growth rate were the result of rapid glycolytic flux, as the cells
166 experience low cellular ATP levels in the *pt* strain.

167 Next, we observed the phenotypes of *pfk1m-pt* double mutant strain. The
168 cellobiose consumption profile of a *pfk1m-pt* double mutant was identical to that of the
169 *pt* strain (Figure 2A). However, the growth rate and relative abundance of G6P, F1,6BP
170 and ATP of the *pfk1m-pt* differed from the *pt* strain (Figure 2C,D). In fact, their levels
171 were similar to those in the *pfk1m* strain. These results imply that while the ATP might
172 be hydrolyzed rapidly due to the *pt* effect, the removal of ATP inhibition on *pfk1* allowed
173 enough ATP to be regenerated downstream that no growth burst was observed. The
174 underlying explanation of the mixed phenotypes will require future experiments to
175 dissect how Pfk1 exerts allosteric control on glycolysis and ATP levels.

176

177 **Carbon starvation-like state of the plasma membrane ATPase**

178 Although cellobiose theoretically provides the same energy and carbon
179 availability to cells as glucose, its releases glucose only after intracellular hydrolysis by
180 β-glucosidase. Thus the cellobiose consumption system used here does not generate
181 extracellular glucose, which acts as a crucial signaling molecule for yeast carbon

182 metabolism. Taken together with the observation that increased ATPase activity in the
183 *pt* strain increased cellobiose consumption efficiency, we wondered whether the limited
184 Pma1 activity in cellobiose-fed cells is due to the absence of extracellular glucose in the
185 media. Transcriptionally, the presence of glucose increases *PMA1* mRNA levels by 2-4
186 times via the regulation of Rap1, Gcr1 and Sir2 (15-17). Consistent with the requirement
187 for extracellular glucose sensing, previous RNA sequencing experiments revealed a
188 40% decrease in *PMA1* transcript levels when cellobiose was provided in place of
189 glucose (5). However, although transcriptional regulation of *PMA1* is important, it is
190 slower than post-transcriptional regulation and results in smaller changes (13, 18).
191 In the presence of glucose, phosphorylation of Ser-899 decreases Pma1's K_m
192 and Ser-911/Thr-912 increases Pma1's V_{max} for ATP, respectively (13, 19, 20). Given
193 the 6-fold excess amount of ATP observed in cellobiose utilizing conditions (Figure 1A),
194 the effective velocity of the Pma1 reaction is likely approaching V_{max} regardless of the
195 phosphorylation status at Ser-899 (21). The K_m of ATP hydrolysis by Pma1 has been
196 reported to increase approximately 3-fold from 1.2 mM in glucose-fermenting cells to 4.0
197 mM in glucose-starved cells, while a 10-fold decrease in V_{max} was reported in the same
198 study (22). We reasoned that the 6-fold increase of ATP in cellobiose-fed cells should
199 result in ATP concentrations in excess of the K_m for Pma1, resulting in Pma1 activity
200 being limited by its V_{max}. Thus, in this study, we did not investigate the phosphorylation
201 of Ser-899 and chose to investigate whether V_{max}-determining phosphorylation states of
202 Ser-911 and Thr-912 might play a major role in establishing the efficiency of cellobiose
203 fermentation (Figure 3A).

204 Combinatorial mutations of Ser-911/Thr-912 to alanine and aspartic acid were
205 introduced into the endogenous *PMA1* gene to prevent or mimic phosphorylation,
206 respectively. We were unable to obtain strains with *pma1*-S911A/T912A and *pma1*-
207 S911A/T912D, potentially because the combinations were lethal. All mutant strains
208 whose Pma1 S911 position was mutated to aspartic acid consumed cellobiose more
209 efficiently in comparison to when the S911 position remained unchanged (Figure 3B).
210 By contrast, mutating Pma1 T912 to aspartic acid did not show a correlation with the
211 cellobiose consumption phenotype. These results suggest that phosphorylation of Pma1
212 at S911 was lacking when cellobiose was provided as a sole carbon source.
213
214 **Positive effects of extracellular glucose sensor deletions**
215 According to the above mutational analysis, the Pma1 phosphorylation state of
216 cellobiose-fed cells was similar to that in carbon starvation conditions (Figure 3A) (20).
217 In the previously published experiments (20), carbon-starved cells were prepared by
218 incubating mid-exponential phase cells in media without glucose. In such conditions,
219 neither extracellular nor intracellular glucose is present. For the cellobiose-fed cells,
220 based on the relatively high level of intracellular glucose we detected (Figure 1A), it is
221 unlikely that the intracellular glucose induced Pma1 carbon starvation. Additionally,
222 since intracellular glucose metabolism is expected in cellobiose-fed cells, its effect on
223 Pma1 carbon starvation was also ruled out (23). We therefore tested the role of
224 extracellular glucose in regulating Pma1 activity. In cellobiose-fed cells, glucose is not
225 provided as part of the media, and thus the extracellular glucose is absent. We

226 hypothesize that the extracellular glucose is likely essential for full activation of Pma1
227 through S911 phosphorylation.

228 Snf3, Rgt2 and Gpr1 are the three known sensors of extracellular glucose in *S.*
229 *cerevisiae*. Snf3 and Rgt2 mainly regulate glucose transport while Gpr1 controls cell
230 physiology via an interaction with Gpa2 to activate protein kinase A and cAMP synthesis
231 (23). To mimic the presence of extracellular glucose, constitutively active mutations
232 (*snf3* R229K, *rgt2* R231K and *gpa2* R273A) were introduced into the endogenous loci to
233 probe the role of each glucose-sensing pathway (24, 25). Surprisingly, the cellobiose
234 consumption efficiency of all the three mutant strains decreased by ~25% (Figure S2A).
235 We then inverted the genetic modifications by deleting *SNF3, RGT2* and/or *GPA2*.
236 Notably, the triple glucose-sensing deletion strain (*snf3*Δ*rgt2*Δ*gpa2*Δ, *or srg*Δ) showed a
237 275% increase in E_c (Figure 4A).

238 Combinatorial deletions revealed that the Gpr1 pathway did not contribute to
239 improved cellobiose fermentation, but combining the *SNF3* and *RGT2* deletions (*sr*Δ)
240 was necessary and sufficient to replicate the E_c of the triple deletion strain (Figure 4A,
241 Figure S2B, C). Consistent with the observed E_c values, the intracellular ATP levels of
242 *srg*Δ and *sr*Δ decreased by 41% and 18% respectively, while those in the individual-
243 deletion strains *snf3*Δ and *rgt2*Δ remained unchanged (Figure 4A). These results reveal
244 a negative correlation between E_c and cellular ATP levels (Figure 4B) and that Snf3 and
245 Rgt2 acted together to regulate cellular ATP levels, in addition to regulating glucose
246 transport.

247 Although the additional deletion of *GPA2* (*gpa2*Δ) in the *sr*Δ strain did not further
248 improve E_c (Fig 4A), it reduced the relative abundance of ATP by 28%, implying that the

249 Gpr1 pathway has a separate mechanism to control cellular ATP levels that does not
250 directly affect carbon metabolism. Consistently, *gpa2*Δ had a negative or neutral impact
251 on cellobiose consumption (Figure S2). The decrease in ATP level may be a result of
252 altered cellular activities, controlled by Gpr1 via the Tor and cAMP-PKA-Ras pathways
253 (23). The relationship between Gpr1-regulated ATP levels and carbon metabolism
254 remains to be discovered. Since *gpa2*Δ did not have a direct effect on E_c, it was not
255 investigated further in this study.
256
257 **Snf3/Rgt2 regulation of cellular ATP levels**
258 To examine whether Snf3/Rgt2 regulated the cellular ATP level in cellobiose
259 fermentations via Pma1, an *snf3*Δ *rgt2*Δ *pma1*-Δ*916* strain (*sr*Δ-*pt*) was constructed.
260 Notably, the E_c of the *sr*Δ-*pt* strain increased more than 4 times in comparison to the
261 wild-type control (Figure 4A, Figure 5A). The improvement was additive, within the
262 range of the ΔE_c summation of *sr*Δ and *pma1*-Δ*916* strains relative to wild-type (Figure
263 5A). Although ATP levels decreased in a nearly linear fashion as a function of E_c (Figure
264 4B), it is not presently possible to ascertain whether the *sr*Δ and *pma1*-Δ*916* mutations
265 act entirely independently due to limitations in measurement accuracy (Figure 5A).
266 To further determine the relationship between Snf3/Rgt2 and Pma1, the
267 vanadate-specific ATPase activity of Pma1 (26) from different strains consuming
268 cellobiose was analyzed (Figure 5B). Consistent with the constitutively active nature of
269 the *pt* mutation, the activities of Pma1 in the *pt* and *sr*Δ-*pt* strains were higher than
270 those observed in the WT or *sr*Δ strains, respectively. Addition of *sr*Δ decreased the
271 Pma1 ATPase activities by 25% and 32% in WT and *pt* strains, respectively. In other

272 words, the absence of Snf3 and Rgt2 led to a partial decrease in Pma1 ATPase activity,
273 which implied that Snf3/Rgt2 partially activated Pma1 ATPase activity in the absence of
274 glucose.
275

276 Discussion

277 To identify the effects of a minimal alteration to carbon metabolism in yeast, we
278 chose a cellobiose-consumption pathway composed of two genes and analyzed its
279 cellular metabolite profiles in comparison to cells provided with glucose, yeast's
280 preferred carbon source (Figure 6). Here we focus on the cellobiose consumption
281 efficiency (E_c), as E_c linearly correlated with ethanol production rate, while ethanol yield
282 remained mostly unchanged (Figure S3).
283 More than half of the metabolites significantly changed in abundance when
284 cellobiose was provided in place of glucose. The buildup of G6P, F6P and ATP in *S.*
285 *cerevisiae* fermenting cellobiose suggested that Pfk1 was one of the bottlenecks in the
286 process. Pfk1 is subjected to complex allosteric regulation, including inhibition by ATP
287 and activation by AMP and fructose 2,6-bisphosphate (F2,6BP) (8-10). The Pfk1
288 bottleneck was partially relieved in cells expressing an ATP/AMP/F2,6BP-insensitive
289 *PFK1* allele, while the ATP level remained elevated. These results contrast with
290 previous studies that identified ATP depletion and the buildup of fructose-1,6-
291 bisphosphate–the metabolite immediately downstream of Pfk1–as a weak link in
292 glycolysis (1). Although we did not investigate the effect of AMP and F2,6BP activation
293 since their changes between glucose and cellobiose conditions were less than 2 fold

294 and they did not meet the significance threshold of a p-value less than 0.01, it is
295 possible that they could influence cellobiose consumption efficiency.
296 ATP is central to a cell's energy currency, but too much ATP is not necessary
297 beneficial (27, 28). In fact, we observed a negative correlation between cellular ATP
298 levels and cellobiose consumption efficiency (Figure 4B). A similar correlation has been
299 reported for glucose as a carbon source, suggesting metabolic uncoupling of energy
300 homeostasis in yeast cells (29). We propose that intracellular glucose concentrations–
301 generated by cellobiose hydrolysis in our experiments–and glucose metabolism (23) are
302 insufficient to trigger glucose activation of key metabolic pathways and enzyme activity.
303 For example, we found that the ATP-dependent proton pump Pma1 existed in a carbon-
304 starvation like state during cellobiose fermentation, and was partially responsible for the
305 aberrant accumulation of ATP. These results suggest that neither intracellular glucose
306 nor glucose metabolism are sufficient to fully activate Pma1. A previous study showed
307 the lack of phosphorylation of S899 and S911/T912 in Pma1, in a
308 hexokinase/glucokinase deletion strain (*hxk1*Δ *hxk2*Δ *glk1*Δ) provided with glucose,
309 suggesting that phosphorylation of these residues requires glucose metabolism (30).
310 Together with our results, we propose that the activation of Pma1 through S911
311 phosphorylation requires both extracellular glucose and glucose metabolism. Our
312 results reveal that the cellobiose utilization system allows uncoupling of glucose
313 metabolism and intracellular glucose from extracellular glucose signaling. Future
314 experiments will be required to reveal why ATP was not consumed by other cellular
315 processes triggered under starvation (31).

316 Cytosolic pH is also a key regulator of carbon utilization (32), and is likely to be
317 impacted by the use of the proton symporter CDT-1 for cellobiose import and the
318 resulting low activity of Pma1. High cytosolic pH is necessary and sufficient to activate
319 Tor-Ras-PKA activities, which are downstream of Gpr1 glucose sensing pathway (32).
320 By contrast, the proton symporter CDT-1 and low activity of Pma1 may result in a low
321 cytosolic pH. However, cytosolic pH alone is unlikely to determine the cellobiose
322 consumption efficiency (E_c) as the strain with an ATP/AMP/F2,6BP-insensitive *PFK1*
323 allele showed improved E_c but unaltered cellular ATP levels. Furthermore, the
324 inactivation of the Gpr1 pathway resulted in decreased cellular ATP but unaltered E_c.
325 Glucose storage, i.e. in the form of trehalose, may be interconnected through the Gpr1
326 pathway because Ras-cAMP activates trehalase required to break down trehalose—a
327 phenomenon observed when gluconeogenesis is switched to glycolysis (33). Trehalose
328 cycling has been shown to lead to an imbalanced state of glycolysis (1). The
329 relationship between carbon storage and E_c will require future studies to examine this
330 relationship.

331 We also found that the well-studied extracellular glucose sensors Snf3/Rgt2
332 exhibited a novel role in cellular ATP homeostasis partially through the major plasma
333 membrane ATPase Pma1. Deletion of extracellular glucose sensors (Snf3/Rgt2)
334 increased cellobiose consumption efficiency and partially restored ATP levels.
335 Interestingly, the absence of the Snf3/Rgt2 decreased Pma1 ATPase activities, an
336 effect that should have led to an increase in ATP level. The restored low ATP level
337 observed in the *sr*Δ strain implied that Snf3/Rgt2 regulated cellular ATP level with
338 additional mechanism(s) other than through Pma1. It is known that deletion of *SNF3*

339 and *RGT2* slows down glucose consumption (34), due to the inability of these strains to
340 degrade Mth1/Std1, which block the promoter regions of hexose transporters required
341 for optimal glucose import (35-38). Unlike glucose, cellobiose does not signal Mth1
342 degradation even with intact Snf3/Rgt2 (38). Thus, genes downstream of Mth1
343 regulation, including hexose transporters, are not expected to be responsible for the
344 improved E_c and decreased cellular ATP levels observed in *sr*Δ. Consistent with this
345 model, no growth defect is observed in a *mth1*Δ strain growing on glucose, suggesting
346 that Snf3/Rgt2 has additional regulatory nodes other than Mth1 (34). Future
347 transcriptional profiling and ribosome profiling experiments will be required to reveal the
348 additional Snf3/Rgt2 roles in cellular ATP homeostasis.

349 The present systems-level study of a minimal synthetic biology pathway for
350 cellobiose consumption revealed the dramatic impact of decoupling extracellular and
351 intracellular glucose sensing, resulting in an overabundance of ATP in cells. The
352 inability of *S. cerevisiae* to catabolize ATP for cellular processes in the presence of
353 intracellular glucose and glucose metabolism but in the absence of extracellular glucose
354 resulted in slow fermentation. Thus, ATP levels must be kept in a relatively narrow
355 range for optimal fermentation and to allow robust startup of glycolysis, yet yeast seems
356 to lack a direct mechanism to monitor ATP concentrations. For example, a dynamic
357 model showed that a small concentration difference of inorganic phosphate, a product
358 of ATP hydrolysis, could alter cell fate from a stable glycolytic steady state to an
359 imbalanced dead-end state (1). Here, we found that the extracellular glucose sensing by
360 Snf3/Rgt2 required for optimal glucose fermentation (2) can be uncoupled from the role
361 of these receptors in regulating ATP homeostasis under carbon starvation conditions. It

362 will be important in the future to map the fully regulatory pathways of ATP homeostasis
363 leading from Snf3/Rgt2 and, independently, terminating in Pma1.
364

365 Materials & Methods

366

367 Yeast strains, media and anaerobic fermentation

368 The *S. cerevisiae* background strain used in this study was S288C *ura3::*P_{PGK1}-
369 *cdt-1* N209S/F262Y-T_{ADH1} *lyp1::*P_{TDH3}*-gh1-1 (codon optimized)-*T_{CYC1} derived by
370 chromosomal DNA library selection (39). The strain was subjected to further
371 modifications using the CRISPRm system (39). The list of strains constructed,
372 CRISPRm guides and primers used are included in Table S1.
373 Seed cultures for cellobiose fermentation experiments were grown in 20 g/L
374 glucose modified optimal minimal media (oMM) (5) and harvested at mid-log phase. All
375 cellobiose fermentation experiments were conducted under strict anaerobic conditions,
376 in 80 g/L cellobiose oMM media at an initial OD_{600} of 20, using 10 mL serum flasks
377 containing 5 mL fermentation in 2-5 biological replicates. The flasks were incubated at
378 30°C, 220 rpm. The cellobiose consumption efficiency (E_c) was defined as the inverse
379 of the area under the curve of extracellular cellobiose concentration over time.
380

381 Analytical analysis of yeast metabolites

382 Extracellular cellobiose concentrations were determined by high performance
383 liquid chromatography on a Prominence HPLC (Shimadzu, Kyoto, Japan) equipped with

384 Rezex RFQ-FastAcid H 10 x 7.8 mm column. The column was eluted with 0.01 N of
385 H_2SO_4 at a flow rate of 1 mL/min, 55°C.
386 For the metabolite profiling comparison between glucose and cellobiose
387 (modified from (40)) , equal amounts of yeast cells at mid-exponential phase of
388 anaerobic sugar consumption (10 g/L cellobiose or glucose) were harvested (final pellet
389 OD_{600} equivalent to 5). The samples were quenched in 180 µL of 40:40:20
390 acetonitrile:methanol:water. Following the addition of 10 nmols of d3 serine (as an
391 internal standard), the mixtures were vortexed and centrifuged at 13,000 rpm for 10
392 minutes. The supernatants were injected onto an Agilent 6460 QQQ LC-MS/MS and the
393 chromatography was achieved by normal phase separation with a Luna NH_2 column
394 (Phenomenex) starting with 100% acetonitrile with a gradient to 100% 95:5 water
395 acetonitrile. 0.1% formic acid or 0.2% ammonium hydroxide with 50 mM ammonium
396 acetate was added to assist with ionization in positive and negative ionization mode,
397 respectively. Five biological replicates were used for each sample analyzed.
398 For targeted intracellular metabolite comparisons, yeast cells equivalent to 20
399 OD_{600} units were harvested and filtered through a 0.8 µm nylon membrane, prewashed
400 with 3 mL water, followed by another 3 mL water wash after cell filtration. The
401 membranes were placed in 1.5 mL extraction solution (0.1 M formic acid, 15.3 M
402 acetonitrile) flash-frozen in liquid nitrogen, and stored at -80°C. Before analysis, the
403 extracts were vortexed for 15 minutes and centrifuged to collect the supernatants at 4°C.
404 Glucose 6-phosphate and fructose 1,6-bisphosphate were separated and identified
405 using a 1200 Series liquid chromatography instrument (Agilent Technologies, Santa
406 Clara, CA). 1 µL of each sample was injected onto an Agilent Eclipse XDB-C18 (2.1 mm

407 i.d., 150 mm length, 3.5 μm particle size) column with a Zorbax SB-C8 (2.1 mm i.d.,
408 12.5 mm length, 5 μm particle size) guard column and eluted at 25 °C and a flow rate of
409 0.2 mL/min with the following gradient (modification from (41)): 15 min isocratic 100%
410 buffer A (10 mM tributylamine/15 mM acetic acid), then in 15 min with a linear gradient
411 to 60% buffer B (methanol), 2 min isocratic 60% B, then 10 min equilibration with 100%
412 buffer A. The eluent from the column was introduced into a mass spectrometer for 25
413 minutes after the first 10 minutes. Mass spectrometry (MS) was performed on an LTQ
414 XL ion trap instrument (Thermo Fisher Scientific, San Jose, CA) with an ESI source
415 operated in negative ion mode. The MS settings were capillary temperature 350 °C, ion
416 spray voltage 4.5 kV, sheath gas flow: 60 (arbitrary units), auxiliary gas flow 10
417 (arbitrary units), sweep gas flow 5 (arbitrary units). For the MS/MS product ion scan, the
418 scan range was m/z 80 to m/z 300. The compounds G6P at m/z 259.1 and F16BP at
419 m/z 339.1 were isolated with an m/z 2 isolation width and fragmented with a normalized
420 collision-induced dissociation energy setting of 35% and with an activation time of 30
421 ms and an activation Q of 0.250.

422 The significance threshold between cells provided with cellobiose and cells
423 provided with glucose was set at a p-value of 0.01. Five biological replicates were used
424 in each sample group. Only the metabolites with higher than a 2 fold-change between
425 each sample group were included in the analysis.

426

427 **Plasma membrane isolation**

428 Strains were subjected to cellobiose fermentation under anaerobic conditions.
429 Yeast cells with an OD_{600} equivalent to 40 were harvested at mid-log phase and flash

430 frozen in liquid nitrogen. Membrane fractions were extracted based on the protocol
431 published in (42).
432
433 **Pma1 ATPase activity assay**
434 The ATPase assay described in (26) was modified as follows. 30 µg of the
435 isolated membrane fraction was incubated in assay buffer (50 mM MES pH 5.7, 10 mM
436 $MgSO_4$, 50 mM KCl, 5 mM NaN_3, 50 mM KNO_3) with and without 3 mM orthovanadate
437 for 25 minutes at 30 °C. 1.8 mM ATP was added to start the 100 uL reactions. The
438 reactions were incubated at 30 °C for 15 minutes, then the membranes were isolated
439 from the reactions by centrifugation at 13,000x g for 10 minutes at 4°C. The released
440 inorganic phosphate was measured in the supernatant using the ATPase/GTPase
441 Activity Assay Kit (Sigma-Aldrich) based on the manufacturer's protocol. The specific
442 Pma1 ATPase activities were calculated by subtracting the concentration of released
443 inorganic phosphate in reactions provided with orthovanadate from those without.
444
445 **Yeast cell-based cellobiose uptake assay**
446 The cell-based cellobiose uptake assay was modified from (43). Yeast strains
447 were grown to mid-exponential phase in 2% oMM glucose, washed with assay buffer (5
448 mM MES, 100 mM NaCl, pH 6.0) three times and resuspended to a final OD_{600} of 10.
449 Equal volumes of the cell suspension and 200 µM cellobiose were mixed to start the
450 reactions, which were incubated at 30°C with continuous shaking for 15 minutes. The
451 reactions were stopped by adding 150 µL of supernatants to 150 µL 0.1 M NaOH. The
452 concentrations of the remaining cellobiose were measured using an ICS-3000 Ion

453 Chromatography System (Dionex, Sunnyvale, CA, USA) equipped with a CarboPac®
454 PA200 carbohydrate column. The column was eluted with a NaOAc gradient in 100 mM
455 NaOH at a flow rate of 0.4 mL/min, 30°C.
456

457 **Acknowledgements**

458 The authors thank Raissa Estrela, Dr. Xin Li, Dr. Ligia Acosta-Sampson, Dr.
459 Yuping Lin and Dr. Matt Shurtleff for helpful discussions. This work was supported by
460 funding from Energy Biosciences Institute to JHDC and from National Institutes of
461 Health (R01CA172667) to DKN.
462

463 **Conflict of Interest**

464 The authors declare that they have no conflict of interest.
465

466 **Author contributions**

467 All authors contributed to the design of the experiments. KC and DIB carried out the
468 experiments. DKN and JHDC aided in interpretation of the systems-level experiments.
469 KC wrote the manuscript, with editing from DIB, DKN, and JDHC.
470

471 ## References:

472 1. **van Heerden JH**, **Wortel MT**, **Bruggeman FJ**, **Heijnen JJ**, **Bollen YJM**,
473 **Planque R**, **Hulshof J**, **O'Toole TG**, **Wahl SA**, **Teusink B**. 2014. Lost in
474 Transition: Start-Up of Glycolysis Yields Subpopulations of Nongrowing Cells.
475 Science **343**:1245114–1245114.

476 2. **Youk H**, **van Oudenaarden A**. 2009. Growth landscape formed by perception
477 and import of glucose in yeast. Nature **462**:875–879.

478 3. **Ha S-J**, **Galazka JM**, **Kim SR**, **Choi J-H**, **Yang X**, **Seo J-H**, **Glass NL**, **Cate JHD**,
479 **Jin Y-S**. 2011. Engineered Saccharomyces cerevisiae capable of simultaneous
480 cellobiose and xylose fermentation. Proc Natl Acad Sci USA **108**:504–509.

481 4. **Galazka JM**, **Tian C**, **Beeson WT**, **Martinez B**, **Glass NL**, **Cate JHD**. 2010.
482 Cellodextrin transport in yeast for improved biofuel production. Science **330**:84–
483 86.

484 5. **Lin Y**, **Chomvong K**, **Acosta-Sampson L**, **Estrela R**, **Galazka JM**, **Kim SR**, **Jin**
485 **Y-S**, **Cate JH**. 2014. Leveraging transcription factors to speed cellobiose
486 fermentation by Saccharomyces cerevisiae. Biotechnology for Biofuels **7**:126.

487 6. **Daran-Lapujade P**, **Rossell S**, **van Gulik WM**, **Luttik MAH**, **de Groot MJL**,
488 **Slijper M**, **Heck AJR**, **Daran J-M**, **de Winde JH**, **Westerhoff HV**, **Pronk JT**,
489 **Bakker BM**. 2007. The fluxes through glycolytic enzymes in Saccharomyces
490 cerevisiae are predominantly regulated at posttranscriptional levels. Proceedings
491 of the National Academy of Sciences **104**:15753–15758.

492 7. **Kim H**, **Lee W-H**, **Galazka JM**, **Cate JHD**, **Jin Y-S**. 2014. Analysis of cellodextrin
493 transporters from Neurospora crassa in Saccharomyces cerevisiae for cellobiose
494 fermentation. Appl Microbiol Biotechnol **98**:1087–1094.

495 8. **Bañuelos M**, **Gancedo C**, **Gancedo JM**. 1977. Activation by phosphate of yeast
496 phosphofructokinase. J Biol Chem **252**:6394–6398.

497 9. **Avigad G**. 1981. Stimulation of yeast phosphofructokinase activity by fructose
498 2,6-bisphosphate. Biochem Biophys Res Commun **102**:985–991.

499 10. **Nissler K**, **Otto A**, **Schellenberger W**, **Hofmann E**. 1983. Similarity of activation
500 of yeast phosphofructokinase by AMP and fructose-2,6-bisphosphate. Biochem
501 Biophys Res Commun **111**:294–300.

502 11. **Rodicio R**, **Strauss A**, **Heinisch JJ**. 2000. Single point mutations in either gene
503 encoding the subunits of the heterooctameric yeast phosphofructokinase abolish
504 allosteric inhibition by ATP. J Biol Chem **275**:40952–40960.

505 12. **Gradmann D**, **Hansen UP**, **Long WS**, **Slayman CL**, **Warncke J**. 1978. Current-
506 voltage relationships for the plasma membrane and its principal electrogenic
507 pump in Neurospora crassa: I. Steady-state conditions. J Membr Biol **39**:333–367.

508 13. **Serrano R**. 1983. In vivo glucose activation of the yeast plasma membrane
509 ATPase. FEBS Lett **156**:11–14.

510 14. **Mason AB**, **Allen KE**, **Slayman CW**. 2014. C-terminal truncations of the
511 Saccharomyces cerevisiae PMA1 H+-ATPase have major impacts on protein
512 conformation, trafficking, quality control, and function. Eukaryotic Cell **13**:43–52.

513 15. **Rao R**, **Drummond-Barbosa D**, **Slayman CW**. 1993. Transcriptional regulation

514 by glucose of the yeast PMA1 gene encoding the plasma membrane H(+)-
515 ATPase. Yeast **9**:1075–1084.

516 16. **García-Arranz M**, **Maldonado AM**, **Mazón MJ**, **Portillo F**. 1994. Transcriptional
517 control of yeast plasma membrane H(+)-ATPase by glucose. Cloning and
518 characterization of a new gene involved in this regulation. J Biol Chem
519 **269**:18076–18082.

520 17. **Kang WK**, **Kim YH**, **Kang HA**, **Kwon K-S**, **Kim J-Y**. 2015. Sir2 phosphorylation
521 through cAMP-PKA and CK2 signaling inhibits the lifespan extension activity of
522 Sir2 in yeast. Elife **4**.

523 18. **Eraso P**, **Mazón MJ**, **Portillo F**. 2006. Yeast protein kinase Ptk2 localizes at the
524 plasma membrane and phosphorylates in vitro the C-terminal peptide of the H+-
525 ATPase. Biochimica et Biophysica Acta (BBA) - Biomembranes **1758**:164–170.

526 19. **Portillo F**, **Eraso P**, **Serrano R**. 1991. Analysis of the regulatory domain of yeast
527 plasma membrane H+-ATPase by directed mutagenesis and intragenic
528 suppression. FEBS Lett **287**:71–74.

529 20. **Lecchi S**, **Nelson CJ**, **Allen KE**, **Swaney DL**, **Thompson KL**, **Coon JJ**,
530 **Sussman MR**, **Slayman CW**. 2007. Tandem phosphorylation of Ser-911 and Thr-
531 912 at the C terminus of yeast plasma membrane H+-ATPase leads to glucose-
532 dependent activation. J Biol Chem **282**:35471–35481.

533 21. **Eraso P**, **Portillo F**. 1994. Molecular mechanism of regulation of yeast plasma
534 membrane H(+)-ATPase by glucose. Interaction between domains and
535 identification of new regulatory sites. J Biol Chem **269**:10393–10399.

536 22. **Goossens A**, **La Fuente de N**, **Forment J**, **Serrano R**, **Portillo F**. 2000.
537 Regulation of yeast H(+)-ATPase by protein kinases belonging to a family
538 dedicated to activation of plasma membrane transporters. Mol Cell Biol **20**:7654–
539 7661.

540 23. **Rolland F**, **Winderickx J**, **Thevelein JM**. 2002. Glucose-sensing and -signalling
541 mechanisms in yeast. FEMS Yeast Res **2**:183–201.

542 24. **Ozcan S**, **Dover J**, **Rosenwald AG**, **Wolfl S**, **Johnston M**. 1996. Two glucose
543 transporters in Saccharomyces cerevisiae are glucose. Proceedings of the
544 National Academy of Sciences **93**:12428–12432.

545 25. **Xue Y**, **Batlle M**, **Hirsch JP**. 1998. GPR1 encodes a putative G protein-coupled
546 receptor that associates with the Gpa2p Galpha subunit and functions in a Ras-
547 independent pathway. EMBO J **17**:1996–2007.

548 26. **Viegas CA**, **Sá-Correia I**. 1991. Activation of plasma membrane ATPase of
549 Saccharomyces cerevisiae by octanoic acid. J Gen Microbiol **137**:645–651.

550 27. **Pontes MH**, **Sevostyanova A**, **Groisman EA**. 2015. When Too Much ATP Is
551 Bad for Protein Synthesis. J Mol Biol **427**:2586–2594.

552 28. **Browne SE**. 2013. When too much ATP is a bad thing: a pivotal role for P2X7
553 receptors in motor neuron degeneration. J Neurochem **126**:301–304.

554 29. **Larsson C**, **Nilsson A**, **Blomberg A**, **Gustafsson L**. 1997. Glycolytic Flux Is
555 Conditionally Correlated with ATP Concentration in. J Bacteriol **179**:7243–7250.

556 30. **Mazón MJ**, **Eraso P**, **Portillo F**. 2015. Specific phospho-antibodies reveal two
557 phosphorylation sites in yeast Pma1 in response to glucose. FEMS Yeast Res.

558 31. **Thomsson E**, **Larsson C**, **Albers E**, **Nilsson A**, **Franzén CJ**, **Gustafsson L**.
559 2003. Carbon starvation can induce energy deprivation and loss of fermentative
560 capacity in Saccharomyces cerevisiae. Appl Environ Microbiol **69**:3251–3257.

561 32. **Dechant R**, **Peter M**. 2014. Cytosolic pH: A conserved regulator of cell growth?
562 Mol Cell Oncol **1**:e969643–4.

563 33. **Thevelein JM**, **Hohmann S**. 1995. Trehalose synthase: guard to the gate of
564 glycolysis in yeast? Trends Biochem Sci **20**:3–10.

565 34. **Choi K-M**, **Kwon Y-Y**, **Lee C-K**. 2015. Disruption of Snf3/Rgt2 glucose sensors
566 decreases lifespan and caloric restriction effectiveness through Mth1/Std1 by
567 adjusting mitochondrial efficiency in yeast. FEBS Lett **589**:349–357.

568 35. **Moriya H**, **Johnston M**. 2004. Glucose sensing and signaling in Saccharomyces
569 cerevisiae through the Rgt2 glucose sensor and casein kinase I. Proceedings of
570 the National Academy of Sciences **101**:1572–1577.

571 36. **Flick KM**, **Spielewoy N**, **Kalashnikova TI**, **Guaderrama M**, **Zhu Q**, **Chang H-C**,
572 **Wittenberg C**. 2003. Grr1-dependent inactivation of Mth1 mediates glucose-
573 induced dissociation of Rgt1 from HXT gene promoters. Molecular Biology of the
574 Cell **14**:3230–3241.

575 37. **Lakshmanan J**, **Mosley AL**, **Ozcan S**. 2003. Repression of transcription by Rgt1
576 in the absence of glucose requires Std1 and Mth1. Curr Genet **44**:19–25.

577 38. **Jouandot D**, **Roy A**, **Kim J-H**. 2011. Functional dissection of the glucose
578 signaling pathways that regulate the yeast glucose transporter gene (HXT)
579 repressor Rgt1. J Cell Biochem **112**:3268–3275.

580 39. **Ryan OW**, **Skerker JM**, **Maurer MJ**, **Li X**, **Tsai JC**, **Poddar S**, **Lee ME**,
581 **DeLoache W**, **Dueber JE**, **Arkin AP**, **Cate JHD**. 2014. Selection of chromosomal
582 DNA libraries using a multiplex CRISPR system. Elife **3**.

583 40. **Benjamin DI**, **Louie SM**, **Mulvihill MM**, **Kohnz RA**, **Li DS**, **Chan LG**, **Sorrentino**
584 **A**, **Bandyopadhyay S**, **Cozzo A**, **Ohiri A**, **Goga A**, **Ng S-W**, **Nomura DK**. 2014.

585 Inositol phosphate recycling regulates glycolytic and lipid metabolism that drives
586 cancer aggressiveness. ACS Chem Biol **9**:1340–1350.

587 41. **Luo B**, **Groenke K**, **Takors R**, **Wandrey C**, **Oldiges M**. 2007. Simultaneous
588 determination of multiple intracellular metabolites in glycolysis, pentose
589 phosphate pathway and tricarboxylic acid cycle by liquid chromatography-mass
590 spectrometry. J Chromatogr A **1147**:153–164.

591 42. **Kaiser CA**, **Chen EJ**, **Losko S**. 2002. Subcellular fractionation of secretory
592 organelles. Meth Enzymol **351**:325–338.

593 43. **Li X**, **Yu VY**, **Lin Y**, **Chomvong K**, **Estrela R**, **Park A**, **Liang JM**, **Znameroski**
594 **EA**, **Feehan J**, **Kim SR**, **Jin Y-S**, **Glass NL**, **Cate JHD**. 2015. Expanding xylose
595 metabolism in yeast for plant cell wall conversion to biofuels. Elife **4**.

596

596 ## Figure Legends

597 **Figure 1. Metabolite profile of cells provided with glucose or cellobiose.** (A)
598 Significant changes of intracellular metabolite levels in cells provided with cellobiose
599 compared to cells provided glucose as a sole carbon source. (B) Schematic
600 representation of metabolite changes. The green and red dots represented higher and
601 lower relative metabolite levels in cells provided with cellobiose compared to cells
602 provided with glucose. Statistical analyses are described in the Materials and Methods.

603 **Figure 2. Manipulation of phosphofructokinase (*PFK1*) and plasma membrane**
604 **ATPase *(PMA1*).** (A) Schematic representation of cellobiose consumption route in the
605 upper glycolytic pathway. Glc, G6P, F6P and ATP are highlighted, and were found in
606 higher abundance when cellobiose was provided in comparison to glucose. (B)
607 Cellobiose consumption profile and (C) cell density profile of the strains with ATP-
608 insensitive Pfk1 (*pfk1m*), constitutively active Pma1 (*pt*) and the combination of both
609 mutations (*pfk1m-pt*) in comparison to the cellobiose pathway-only strain, here used as
610 wild-type (WT). (D) Relative abundance of G6P, F1,6BP and ATP levels of the WT,
611 *pfk1m, pt* and *pfk1m-pt* strains, relative to the WT strain fermenting cellobiose. The
612 experiments were carried out in 5 biological replicates, with standard errors from the
613 mean shown.

614 **Figure 3. Carbon starvation-like state of the plasma membrane ATPase (*PMA1*) in**
615 **cellobiose-fermenting cells.** (A) Phosphorylation states of Pma1 residues S911 and
616 T912 under carbon starvation, glucose metabolizing and cellobiose metabolizing
617 conditions. (B) Cellobiose consumption efficiency (E_c) of cells expressing Pma1 with
618 phosho-mimic or phosphorylation-preventing mutations at positions serine 911 (S911)

619 and threonine 912 (T912). Shown are the mean and standard deviation for 3 biological
620 replicates. The experiments were carried out in 2 biological replicates, with standard
621 errors from the mean shown.

622 **Figure 4. Effect of glucose sensor deletions.** (A) Cellobiose consumption efficiency
623 (E_c) and cellular ATP levels of strains with different glucose sensor deletions and
624 different combinations of constitutively-active Pma1 mutations. Shown are the averages
625 and standard deviations of three biological replicates. (B) Correlation of E_c and cellular
626 ATP. Standard deviations for three biological replicates are shown for each point.

627 **Figure 5. Glucose sensor deletions and cellular ATP levels.** (A) Additive effect of the
628 increase in E_c and the decrease in cellular ATP of *sr*Δ and *pt* in *sr*Δ-*pt* strain. The
629 experiments were carried out in 5 biological replicates, with standard errors form the
630 mean shown. (B) Specific Pma1 ATPase of WT*, pt, sr*Δ and *sr*Δ-*pt* strains measured
631 from normalized membrane fractions of cells harvested at mid-log phase. The
632 experiments were carried out in 3 biological replicates, with standard errors from the
633 mean shown.

634 **Figure 6. Schematic representation of ATP homeostasis and cellular regulation of**
635 **cellobiose fermentation.** Excess ATP inhibited phosphofructokinase (Pfk1), resulting
636 in an upper glycolytic metabolite buildup and slow cellobiose consumption. The buildup
637 of ATP may be caused by low activity of Pma1, with no phosphorylation at position 911.
638 Additionally, glucose sensors Snf3 and Rgt2 together influenced cellular ATP levels via
639 Pma1 and other mechanisms to be identified.

640 **Supplementary Figure legends**

641 **Figure S1. Metabolite profile of cells provided with glucose or cellobiose.** (A) cell
642 density and sugar consumption profiles of the strains used for metabolite profiling
643 experiments. (B) Heatmap representation of steady state intracellular metabolite
644 abundance of cells provided with glucose or cellobiose under anaerobic conditions.
645 Shown are the results of 5 biological replicates. Asterisks (*) mark identified compounds
646 that were significantly different between glucose and cellobiose conditions at a
647 significance threshold of a p-value < 0.01.

648 **Figure S2. Cellobiose consumption profiles and efficiency of Snf3, Rgt2 and Gpa2**
649 **mutants.** (A) Cellobiose consumption profiles of strains with consitutively active Snf3
650 (R229K), Rgt2 (R231K) and Gpa2 (R273A). (B) Cellobiose consumption profiles of
651 *SNF3*, *RGT2*, and *GPA2* double deletion combinations. (C) Cellobiose consumption
652 profiles of *SNF3* and *RGT2* single deletion in comparison to the *srΔ, srgΔ and srΔ-pt*
653 strains. (D) Cellobiose consumption profiles of *GPA2* deletion (*gΔ)* in comparison to the
654 WT strain. In panels A, B, C, and D, the results of 3 biological replicates are shown.

655 **Figure S3. Relationship of ethanol productivity parameters and cellobiose**
656 **consumption efficiency (E_c).** Ethanol production rate and the final concentration of
657 ethanol are plotted against E_c.

658

659

660

660

661 **Table S1:** List of strains constructed, CRISPRm guides and primers.

662

A

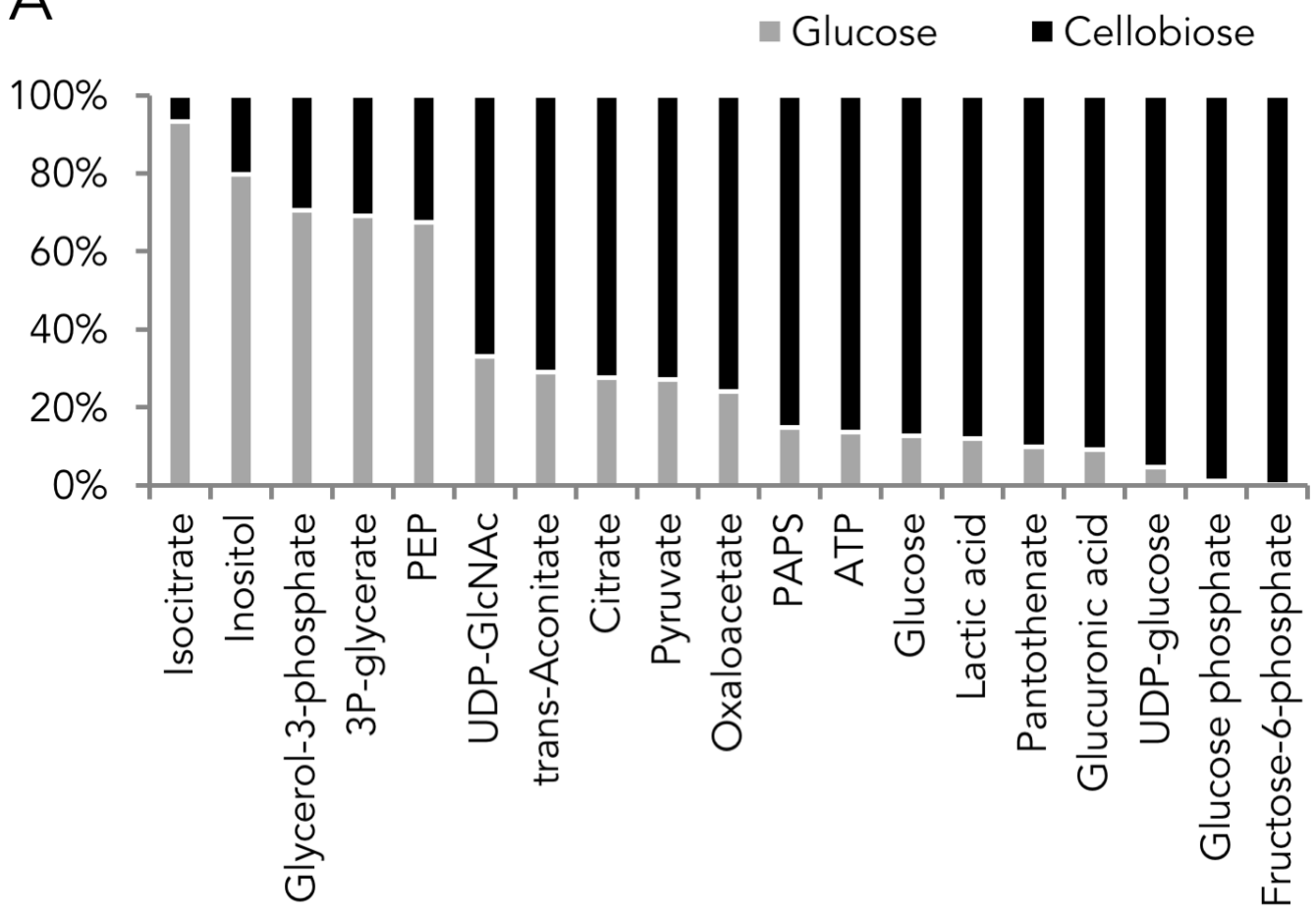
Glucose
Cellobiose
100%
80%
60%
40%
20%
0%
Isocitrate
Inositol
Glycerol-3-phosphate
3P-glycerate
PEP
UDP-GlcNAc
trans-Aconitate
Citrate
Pyruvate
Oxaloacetate
PAPS
ATP
Glucose
Lactic acid
Pantothenate
Glucuronic acid
UDP-glucose
Glucose phosphate
Fructose-6-phosphate

B

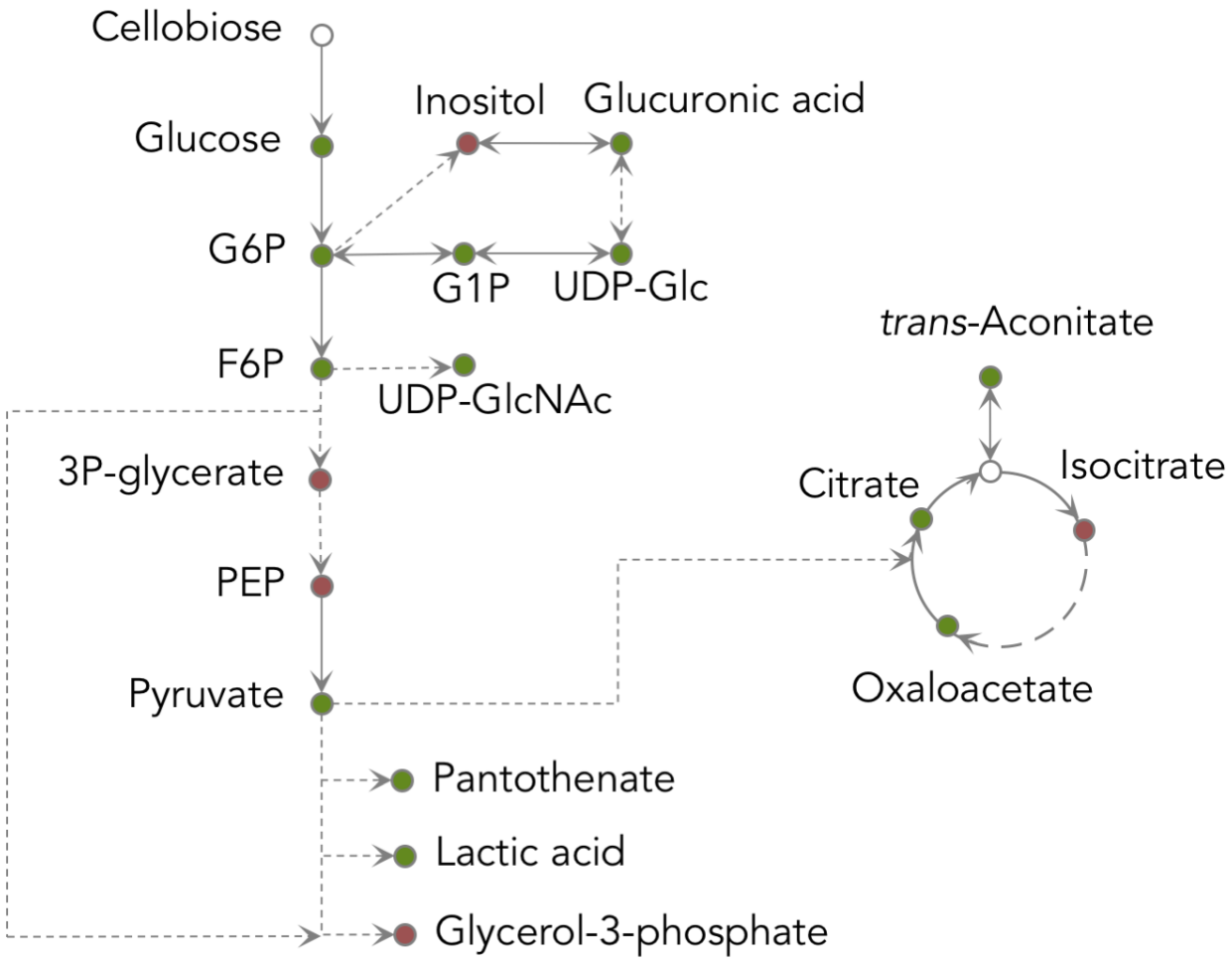
Cellobiose
Glucose
Inositol
Glucuronic acid
G6P
G1P
UDP-Glc
F6P
UDP-GlcNAc
trans-Aconitate
3P-glycerate
Citrate
Isocitrate
PEP
Pyruvate
Oxaloacetate
Pantothenate
Lactic acid
Glycerol-3-phosphate

A

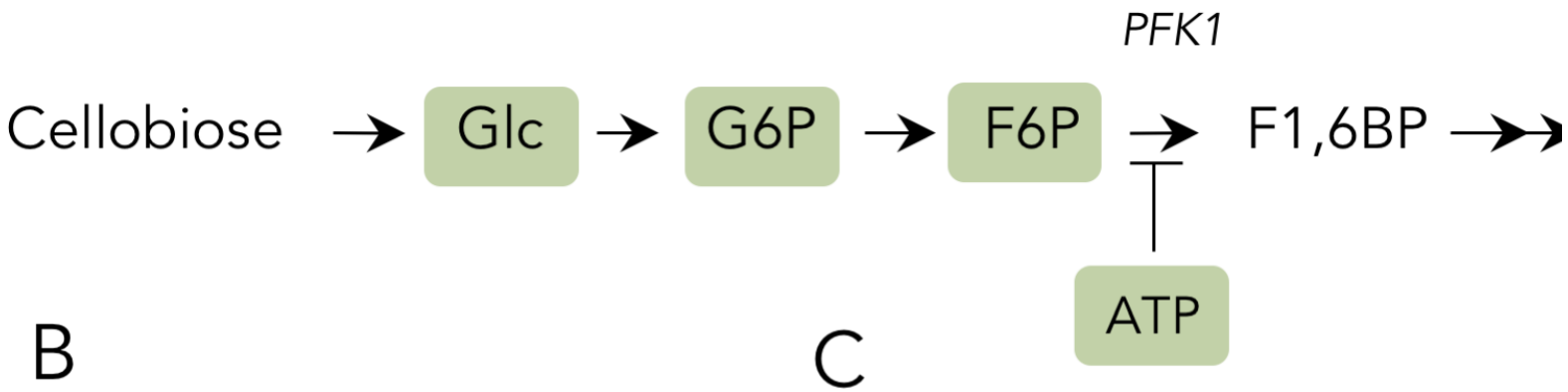
PFK1
Cellobiose
Glc
G6P
F6P
F1,6BP
ATP

B

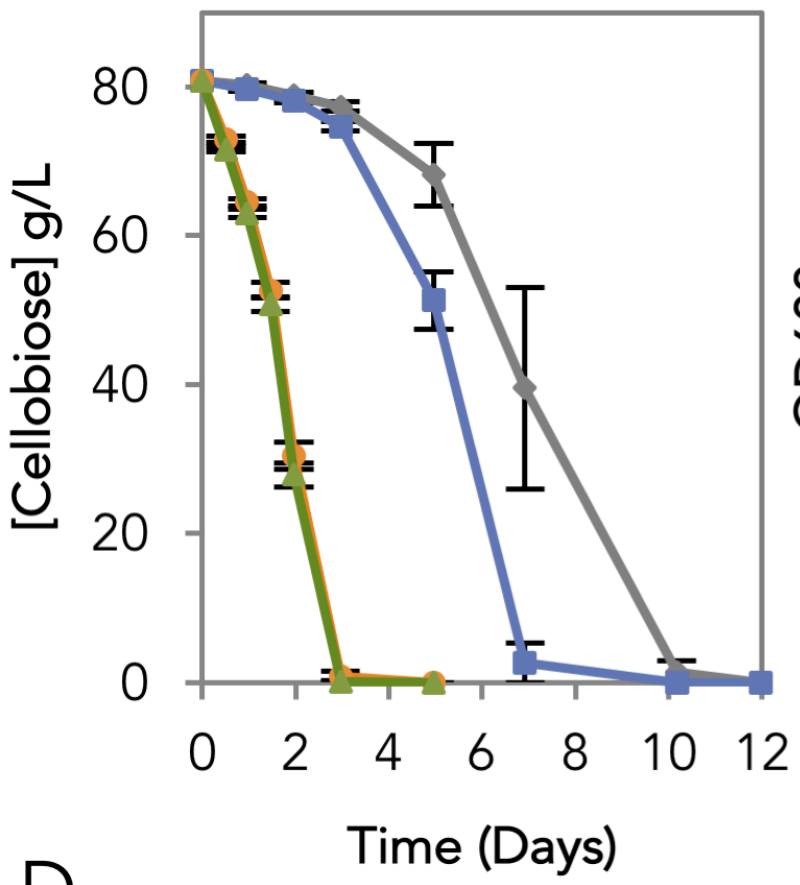
[Cellobiose] g/L
80
60
40
20
0
0
2
4
6
8
10
12
Time (Days)

C

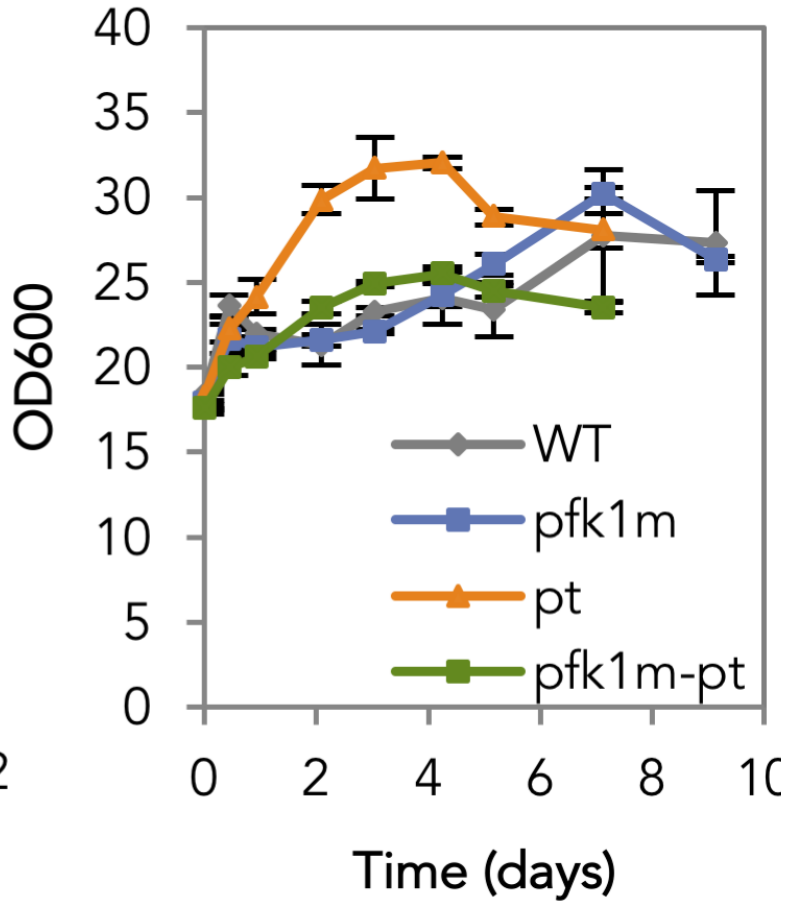
OD600
40
35
30
25
20
15
10
5
0
0
2
4
6
8
10
Time (days)
WT
pfk1m
pt
pfk1m-pt

D

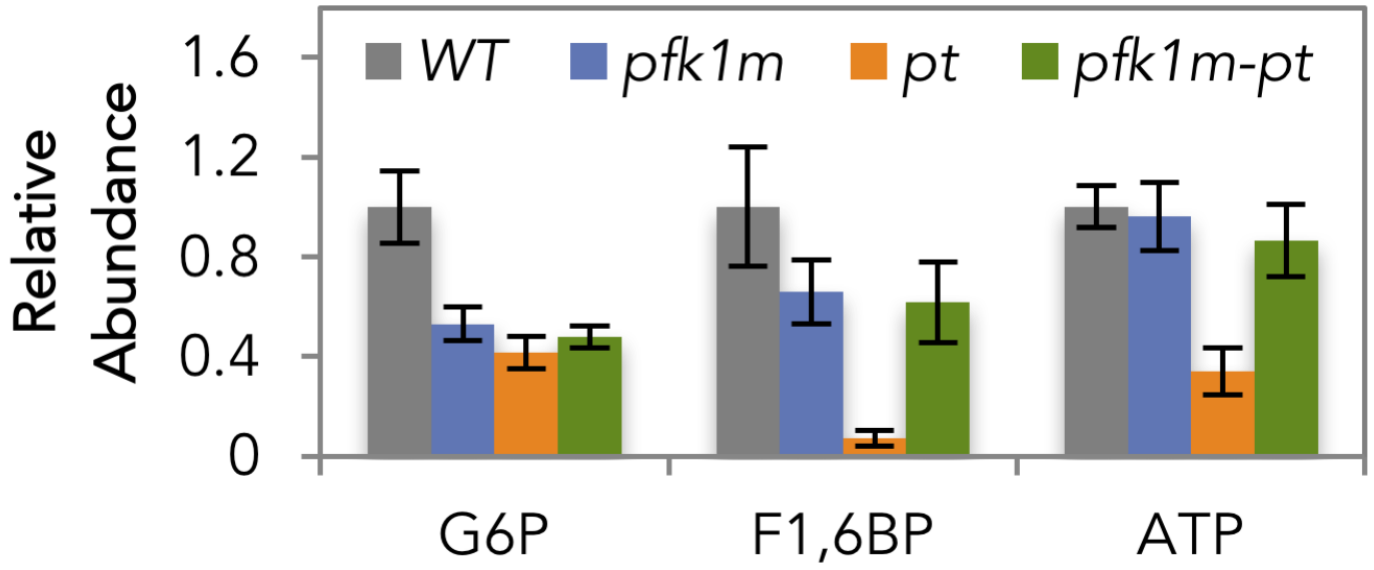
Relative Abundance
1.6
1.2
0.8
0.4
0
WT
pfk1m
pt
pfk1m-pt
G6P
F1,6BP
ATP

A

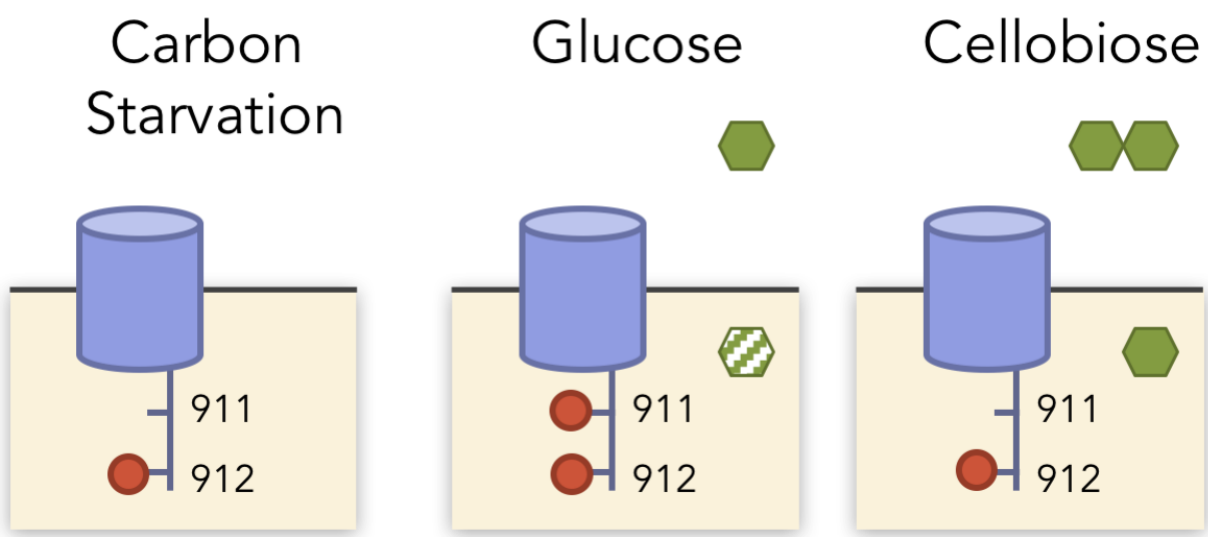
Carbon Starvation
Glucose
Cellobiose
911
912
911
912
911
912

B

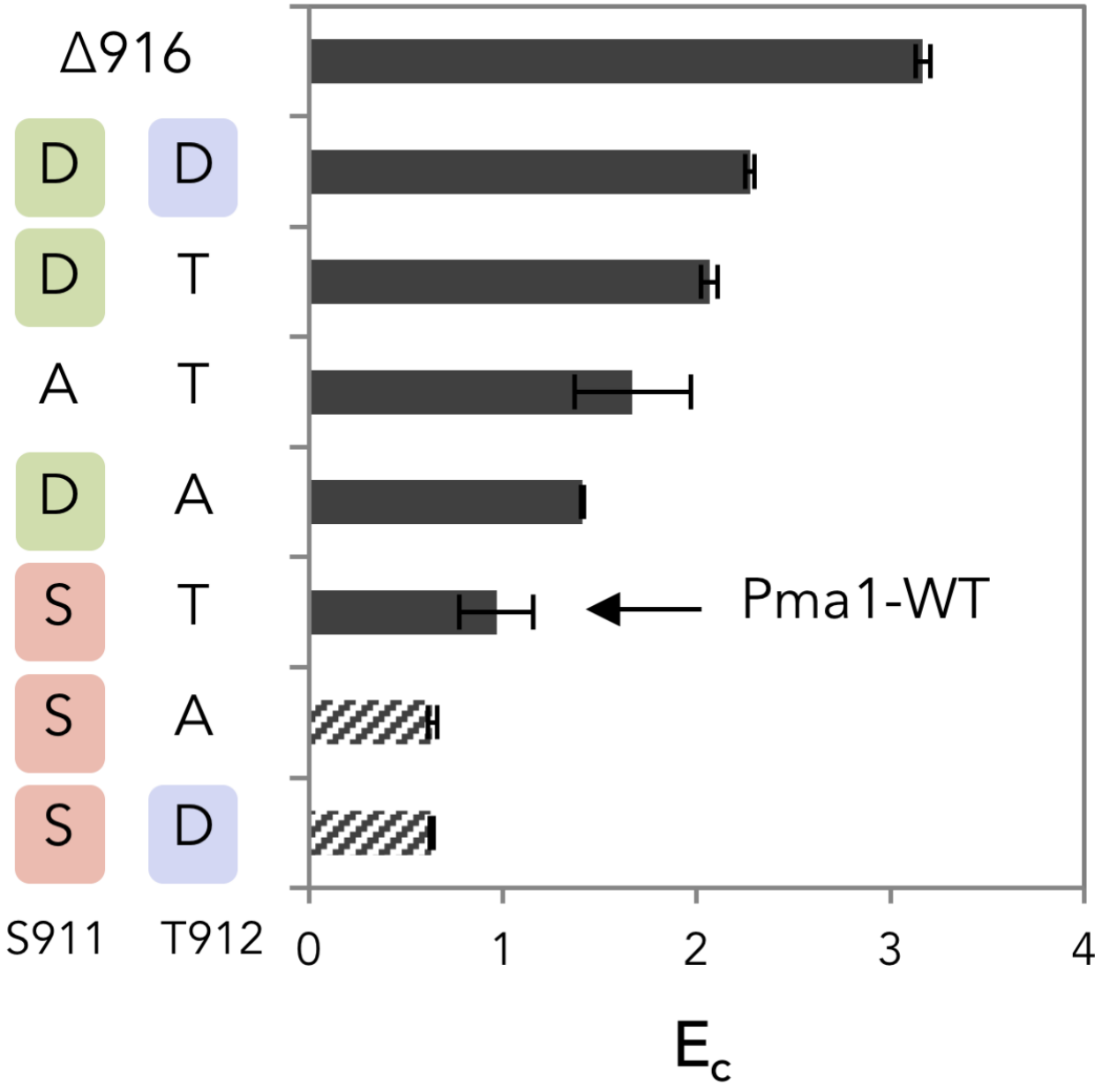
Δ916
D D
D T
A T
D A
S T
S A
S D
S911 T912
Pma1-WT
0
1
2
3
4
E_c

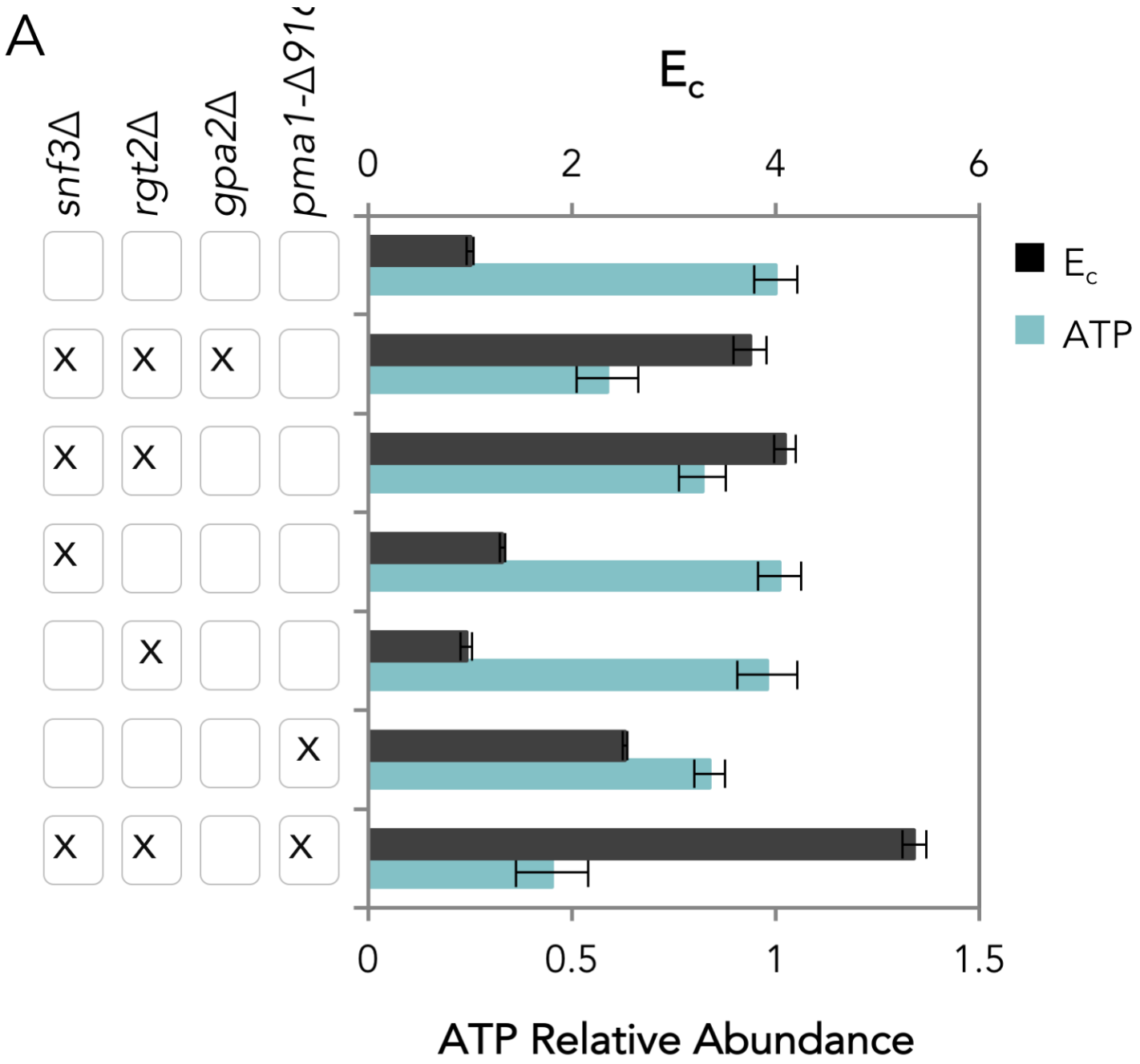
A
snf3Δ
rgt2Δ
gpa2Δ
pma1-Δ91
Ec
0
2
4
6
Ec
ATP
0
0.5
1
1.5
ATP Relative Abundance

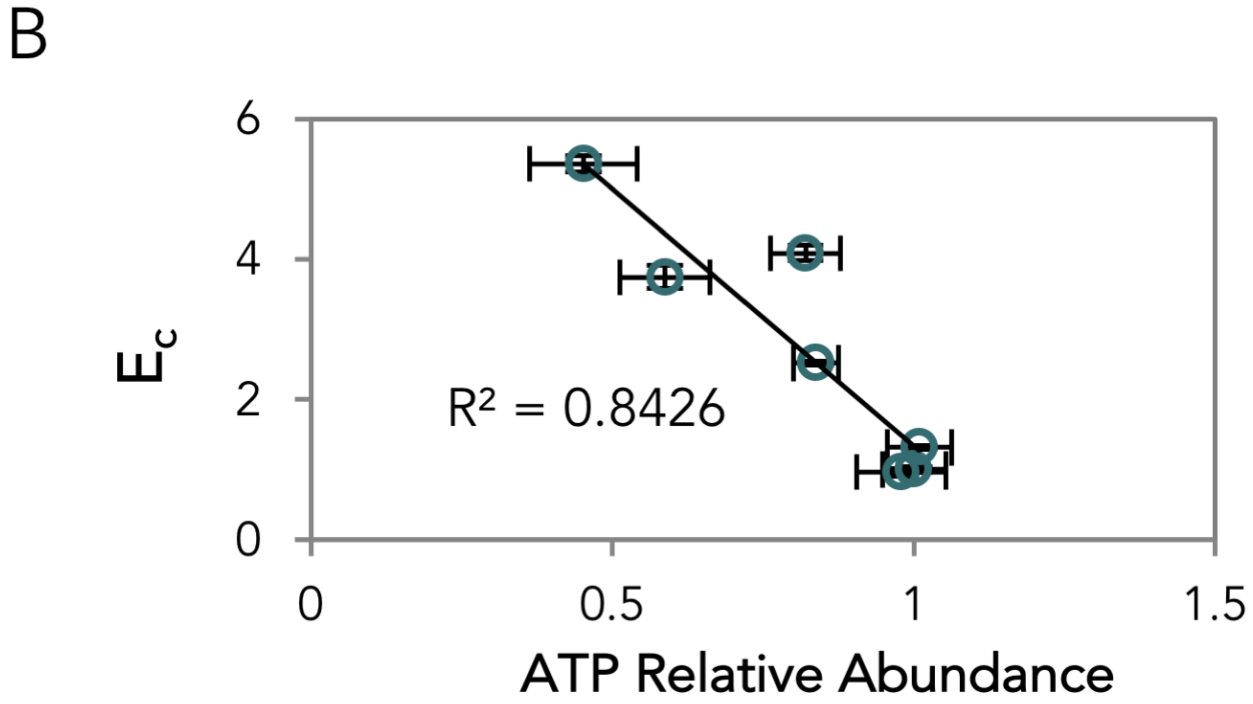
B
6
4
2
0
Ec
R² = 0.8426
0
0.5
1
1.5
ATP Relative Abundance

A

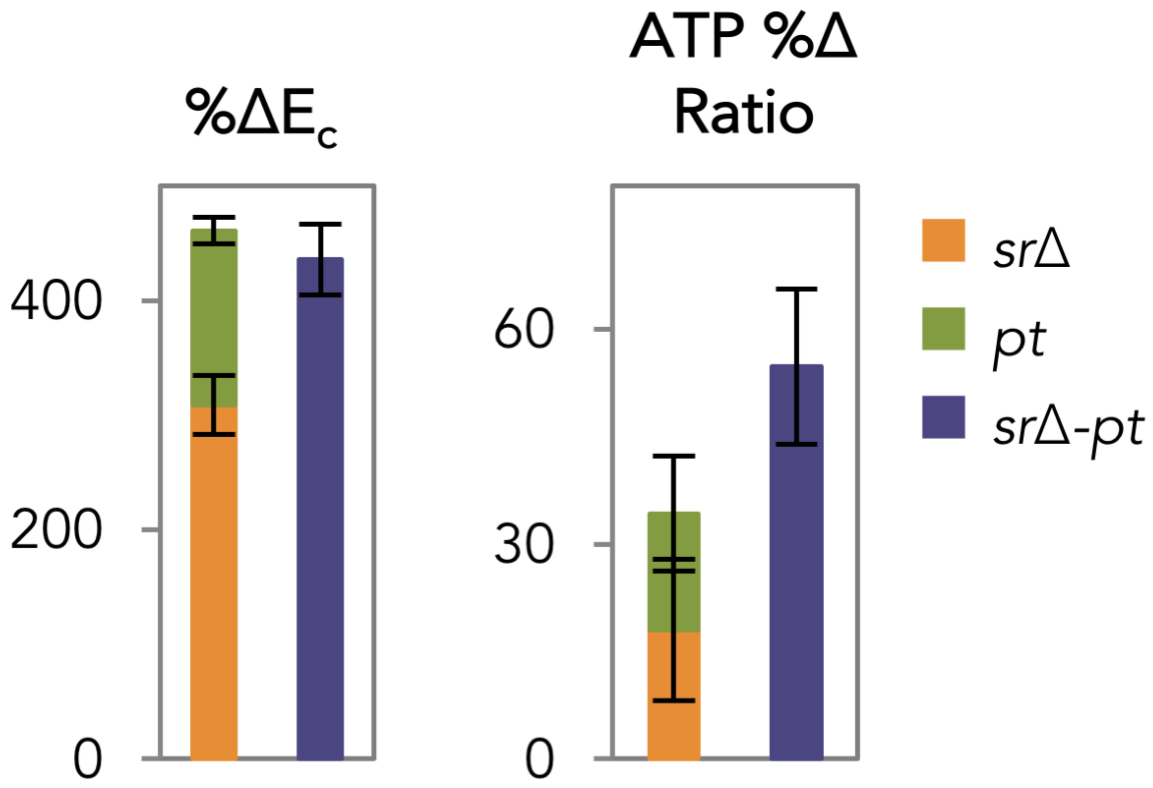
%ΔE$_c$
ATP %Δ Ratio
400
200
0
60
30
0
srΔ
pt
srΔ-pt

B

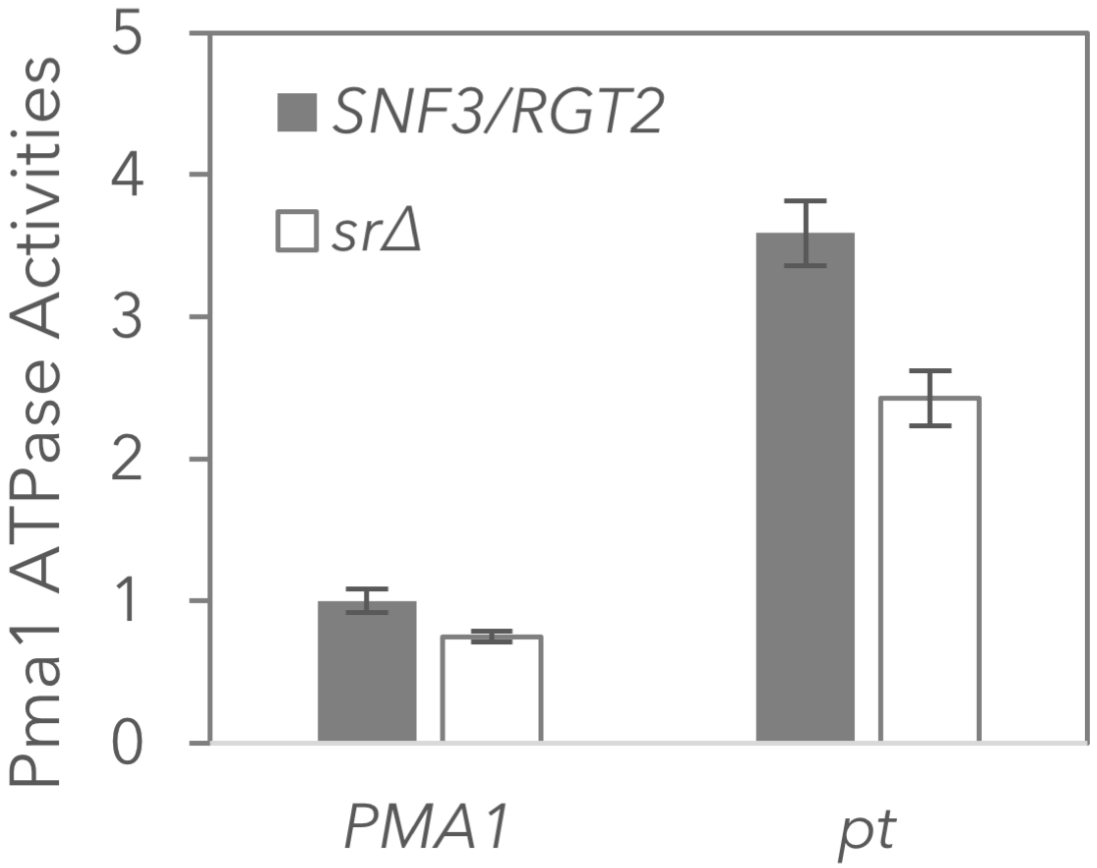
Pma1 ATPase Activities
5
4
3
2
1
0
SNF3/RGT2
srΔ
PMA1
pt

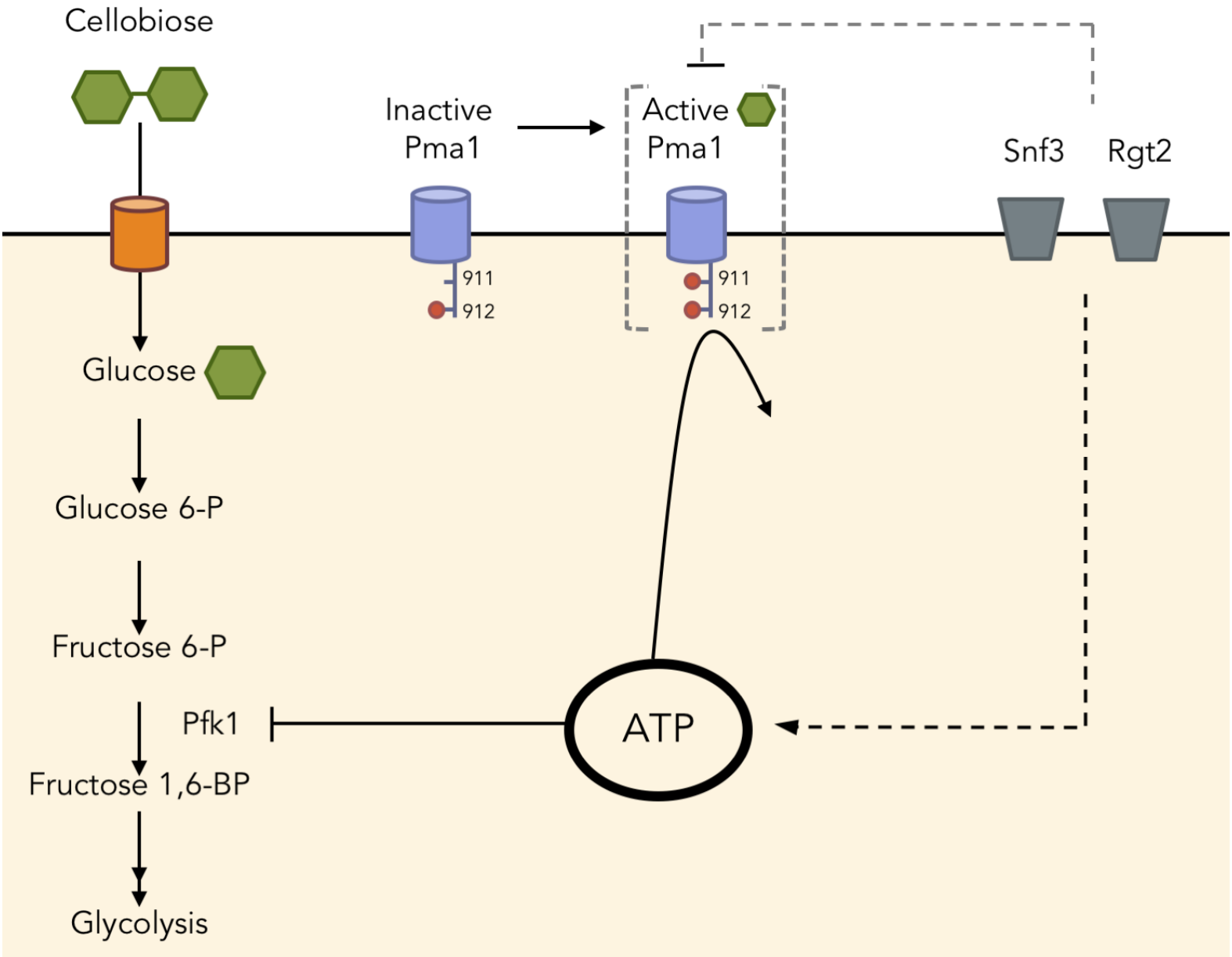
Cellobiose
Inactive
Pma1
Active
Pma1
Snf3
Rgt2
911
912
911
912
Glucose
Glucose 6-P
Fructose 6-P
Pfk1
ATP
Fructose 1,6-BP
Glycolysis